Int. J. Heat Mass Transfer. Vol. 32, No. 6, pp. 1037–1052, 1989
Printed in Great Britain

0017–9310/89 $3.00 + 0.00

Steady laminar heat transfer in the entry region of circular tubes with axial diffusion of heat and momentum

GIORGIO PAGLIARINI

Istituto di Fisica Tecnica, Facoltà di Ingegneria, Università di Bologna,
V. le Risorgimento 2, 1-40136 Bologna, Italy

(*Received* 12 *March* 1988 *and in final form* 1 *July* 1988)

Abstract—The simultaneous development of the velocity and temperature profiles in circular tubes is analysed, accounting for axial diffusion of both momentum and heat. The axisymmetric problem is formulated in variational form by the weighted residuals Galerkin method and then numerically solved by the finite element method. Results obtained in the case of vanishing axial diffusion effects satisfactorily compare with previous boundary layer solutions; in the presence of axial diffusion effects the solutions presented in the literature are scanty and do not always agree. The isothermal flow results, presented for Reynolds numbers ranging from 1 to 1000, show the appearance of the overshoots in the axial velocity profile, as well as the dependence on the axial coordinate and Reynolds number of the various axial momentum transfer processes—radial diffusion at the wall, convection and axial diffusion. The non-isothermal flow results, presented for the Prandtl number ranging from 0.1 to 100 and the Péclet number from 5 to 500, point out the effect of axial diffusion of momentum and, above all, of heat, on the convective heat transfer rate.

INTRODUCTION

AXIAL DIFFUSION of both momentum and heat is usually overlooked in the design and analysis of heat transfer devices. Nevertheless, the first may affect considerably the velocity distribution in low Reynolds number flows; the second, the temperature distribution at low Péclet numbers. Moreover, in the convective heat transfer of low Reynolds number flows, the axial diffusion of momentum may also affect the temperature distribution in the fluid. This is the case of the simultaneous development of temperature and velocity profiles in slow flows. Shah and London [1] reviewed the most relevant bibliography about hydrodynamically and thermally developing flow in their monograph on laminar forced convection in ducts. The distinct analyses of hydrodynamic and thermal entrance problems provide the limits beyond which axial diffusive transport can be neglected with respect to radial diffusive and convective transport. Momentum axial diffusion, as well as radial pressure gradient, can be neglected far from the immediate entrance, providing the Reynolds number is greater than about 400, while axial diffusion of heat can be neglected at Péclet numbers greater than 10 when the wall heat flux is specified as uniform at the boundary, case ⓗ, and greater than 50 when the wall temperature is specified as uniform at the boundary, case ⓣ. Below these limits or near the entrance, axial diffusive transport considerably affects the development of velocity and temperature profiles.

Vrentas *et al.* [2] first showed the effect of momentum axial diffusion in the hydrodynamic entry length problem for an isothermal fluid flowing in a circular tube. Christiansen *et al.* [3] extended this analysis to the presence of an abrupt contraction. Both solved the complete momentum equation in an infinite domain by the finite difference method. The upstream portion of the duct is a stream tube, impermeable and frictionless; the downstream portion is a real tube, with no slip at the tube wall. In the stream tube, away from the entrance, the velocity distribution is uniform. Near the entrance of the real tube, the high axial gradients in the velocity field cause diffusion of momentum upstream. This results in some velocity profile development in the stream tube. Momentum axial diffusion may also affect considerably the velocity profiles in the real tube where, at low Reynolds numbers, it attenuates to disappearance the overshoots which are formed in the axial velocity profile to satisfy the continuity equation near the entrance. A further effect is the increase of the hydrodynamic entrance length as the Reynolds number decreases.

Many other investigators have analysed the hydrodynamic entrance problem by solving the complete momentum equation while assuming a known velocity profile at the inlet. This condition prevents momentum from diffusing upstream; their solutions are therefore of minor relevance for the present paper. Schmidt and Zeldin [4] assumed an initial condition of irrotational uniform velocity in their numerical solution. They showed that the pressure drop in the entrance region lowers with increasing Reynolds number; nevertheless their distributions of the apparent Fanning friction factor–Reynolds number product, tabulated in ref. [1], show different shapes for different Reynolds numbers. Shah and London are not certain

NOMENCLATURE

c	specific heat
C	pressure correction factor, equation (25)
f_{app}	apparent Fanning friction factor, equation (22)
f_m	average Fanning friction factor in the hydrodynamic entry length, equation (23)
h	convective heat transfer coefficient
Ⓗ	thermal boundary condition referring to uniform wall heat flux
k	thermal conductivity
k_x	thermal conductivity in the axial direction
K_a	momentum axial diffusion correction factor, equation (29)
K_d	momentum flux correction factor, equation (24)
L^+_{hy}	dimensionless hydrodynamic entrance length, $L'_{hy}/(2R\,Re)$
L^*_{th}	dimensionless thermal entrance length, $L'_{th}/(2R\,Pe)$
n	dimensionless outer normal to the boundary of the integration domain, n'/R
Nu	Nusselt number, $2Rh/k$
p	dimensionless pressure, $p'/(\rho U^2/2)$
Pe	Péclet number, $Re\,Pr$
Pr	Prandtl number, $v\rho c/k$
q	heat flux
r	dimensionless radial coordinate, r'/R
r_{max}	dimensionless radial position where the maximum increment of the axial velocity component takes place
R	radius of the tube
$\mathbf{R}$	residual of a conservation equation
Re	Reynolds number, $2RU/v$
S	dimensionless boundary surface of the integration domain, S'/R^2
T	temperature
Ⓣ	thermal boundary condition referring to uniform wall temperature
u	dimensionless fluid axial velocity, u'/U
U	fluid mean axial velocity
v	dimensionless fluid radial velocity, v'/U
V	dimensionless volume of the integration domain, V'/R^3
x	dimensionless axial coordinate, x'/R
x^+	dimensionless axial coordinate for the hydrodynamic entrance region, $x'/(2R\,Re)$
x^*	dimensionless axial coordinate for the thermal entrance region, $x'/(2R\,Pe)$
x^+_{max}	dimensionless axial position where the maximum increment of the axial velocity component takes place.

Greek symbols

Δ_{max}	maximum increment of the axial velocity component as a percentage of the centreline value
Θ_H	dimensionless fluid temperature for the Ⓗ thermal boundary condition, $(T-T_e)k/(2Rq_w)$
Θ_T	dimensionless fluid temperature for the Ⓣ thermal boundary condition, $(T-T_w)/(T_e-T_w)$
v	kinematic viscosity
ρ	density.

Subscripts

e	initial value at $x' = -\infty$
fb	fluid bulk
fd	fully developed flow
H	Ⓗ boundary condition
T	Ⓣ boundary condition
w	wall
x	local value.

Superscripts

$'$	dimensional quantity
$\bar{}$	average value over the tube cross-section
$\tilde{}$	trial function.

as to whether this trend is to be attributed to the nature of the finite difference equations and numerical method at startup or to the overshoots in the velocity profile, which for Schmidt and Zeldin's initial conditions are stronger than in the stream tube–real tube model, as the comparison between the results presented in refs. [2, 3] and those of McDonald *et al.* [5] shows.

All of the above analyses involve isothermal flow. The effect of axial heat conduction is particularly shown by the solution of the complete energy equation in an infinite domain. In this paper attention is focused on the thermal entrance problem in circular tubes of infinite extent with wall heat flux or wall temperature specified as uniform at the boundary, while assuming that the upstream portion of the tube is thermally insulated. Hennecke [6] and Verhoff and Fisher [7] applied the finite difference method to this problem, assuming uniform heat flux at the boundary. Hsu [8], Davis [9], Vick *et al.* [10] and Vick and Ozisik [11] analytically analysed the same problem. Papoutsakis *et al.* [12] obtained an analytical solution for the more general problem of a heating section of finite length. Verhoff and Fisher [7] analysed the thermal entrance problem also with the Ⓣ boundary condition. Tan and Hsu [13], Newman [14] and Michelsen and

Villadsen [15] analytically analysed this same problem. For both thermal boundary conditions, at low Péclet numbers, a considerable amount of heat is conducted upstream in the tube not directly heated, thus affecting the temperature distribution at the entrance. As a further effect of axial heat diffusion, the thermal entrance length increases as the Péclet number decreases. For the ⓗ boundary condition, the local Nusselt number decreases near the entrance as the Péclet number decreases, but increases further downstream. Tan and Hsu [13] observed a similar trend also for the ⓣ boundary condition, whereas the Michelsen and Villadsen [15] solution shows that the local Nusselt number increases as the Péclet number decreases, approaching infinity near the inlet. The analysis of Newman [14] confirms this trend. Verhoff and Fisher [7] do not specify any particular trend for the local Nusselt number distribution, while showing by their results a less steep increase towards the inlet. Papoutsakis [16] analysed the behaviour of his analytic solution near the entrance for various combinations of wall boundary conditions. He observed also that for the Neuman boundary condition upstream and the Dirichlet one downstream, the Nusselt number near the entrance of the heating section should be bounded, as in the case of the Neuman boundary condition required all along the tube.

McMordie and Emery [17] analysed the problem of simultaneous development of temperature and velocity profiles in a semi-infinite circular tube accounting for axial heat diffusion with uniform initial temperature and uniform wall heat flux at the boundary. They numerically solved the energy equation, assuming a uniform velocity profile for the initial portion of the inlet region while using the Langhaar [18] solution further downstream. This is a boundary layer-type solution which neglects momentum axial diffusion as well as the radial pressure gradient. Moreover, also within the limits of this idealization, the Langhaar velocity distribution provides a poor approximation, which Hornbeck [19] ascribes to the linearization of the inertia terms in the momentum equation. Owing to the initial condition, their local Nusselt number increases as the Péclet number decreases near the entrance, where it is unbounded. Christiansen and Kelsey numerically analysed the simultaneous hydrodynamic and thermal development of Newtonian [20] and non-Newtonian [21] fluids following an abrupt contraction with the ⓣ boundary condition. However, computational instabilities limited their computations to Reynolds and Péclet numbers of less than 100. The local Nusselt number distributions presented in ref. [21] show that near the entrance, axial diffusion causes the local Nusselt number to approach an upper limit which increases as the Péclet number increases.

The author is unaware of any previous analyses of axial diffusion effects in simultaneously developing flow in circular tubes of infinite extent. Moreover, the axial diffusion of momentum in isothermal flows and of heat in hydrodynamically developed flows requires further analysis, as the results presented in the quoted literature also show.

In this paper, the problem of simultaneously developing flow in a circular tube—accounting for axial diffusion of both momentum and heat—is analysed. The axisymmetric problem is treated numerically by the finite element method, which Ben-Sabar and Caswell [22] have shown to be stable in convection–diffusion transport. The assumption of constant property fluid allows the hydrodynamic and thermal entrance problems to be solved independently. The discrete system of equations in the velocity components, pressure and temperature is obtained by applying the weighted residuals Galerkin method to the conservation equations. The domain of integration is discretized by means of axisymmetric elements having triangular cross-sections. Within each element, the velocity components and temperature are approximated by quadratic polynomials and the pressure by linear polynomials. All the volume and surface integrations in the coefficient matrix, as well as on the right-hand side of the solving system, are performed analytically. The nonlinearity in the momentum equation is handled by an iterative scheme. The systems of linear algebraic equations are then solved by a library subroutine.

BASIC EQUATIONS AND RELEVANT PARAMETERS

The problem analysed in this paper concerns steady laminar flow of a Newtonian constant property fluid through a circular tube of infinite extent. Viscous dissipation is neglected. In the upstream region ($x' < 0$), the wall is impermeable, frictionless and thermally insulated; in the downstream region ($x' > 0$) the wall is real and subject to the boundary condition of uniform wall heat flux or uniform wall temperature. Far upstream the temperature is uniform and the velocity irrotational with a uniform axial component.

By utilizing the dimensionless quantities defined in the Nomenclature, the dimensionless form of the governing equations is as follows:

continuity equation

$$\frac{\partial u}{\partial x}+\frac{\partial v}{\partial r}+\frac{v}{r}=0; \tag{1}$$

momentum equation

axial direction

$$u\frac{\partial u}{\partial x}+v\frac{\partial u}{\partial r}=-\frac{1}{2}\frac{\partial p}{\partial x}+\frac{2}{Re}\left(\frac{\partial^2 u}{\partial r^2}+\frac{1}{r}\frac{\partial u}{\partial r}+\frac{\partial^2 u}{\partial x^2}\right) \tag{2}$$

radial direction

$$u\frac{\partial v}{\partial x}+v\frac{\partial v}{\partial r}=-\frac{1}{2}\frac{\partial p}{\partial r}+\frac{2}{Re}\left(\frac{\partial^2 v}{\partial r^2}+\frac{1}{r}\frac{\partial v}{\partial r}-\frac{v}{r^2}+\frac{\partial^2 v}{\partial x^2}\right); \tag{3}$$

energy equation

$$u\frac{\partial\Theta}{\partial x}+v\frac{\partial\Theta}{\partial r}=\frac{2}{Pe}\left(\frac{\partial^2\Theta}{\partial r^2}+\frac{1}{r}\frac{\partial\Theta}{\partial r}+\frac{\partial^2\Theta}{\partial x^2}\right). \quad (4)$$

For equations (1)–(3) the following boundary conditions are required:

$$u(-\infty,r)=1 \quad 0\leqslant r\leqslant 1 \quad (5)$$

$$\left.\frac{\partial v}{\partial x}\right|_{x=-\infty}=0 \quad 0\leqslant r\leqslant 1 \quad (6)$$

$$u(\infty,r)=2(1-r^2) \quad 0\leqslant r\leqslant 1 \quad (7)$$

$$v(\infty,r)=0 \quad 0\leqslant r\leqslant 1 \quad (8)$$

$$\left.\frac{\partial u}{\partial r}\right|_{r=0}=0 \quad -\infty\leqslant x\leqslant\infty \quad (9)$$

$$v(x,0)=0 \quad -\infty\leqslant x\leqslant\infty \quad (10)$$

$$\left.\frac{\partial u}{\partial r}\right|_{r=1}=0 \quad -\infty\leqslant x<0 \quad (11)$$

$$u(x,1)=0 \quad 0\leqslant x\leqslant\infty \quad (12)$$

$$v(x,1)=0 \quad -\infty\leqslant x\leqslant\infty. \quad (13)$$

For the energy equation, two different boundary conditions are considered:

uniform wall heat flux Ⓗ

$$\Theta_H(-\infty,r)=0 \quad 0\leqslant r\leqslant 1 \quad (14)$$

$$\left.\frac{\partial\Theta_H}{\partial x}\right|_{x=\infty}=\frac{4}{Pe} \quad 0\leqslant r\leqslant 1 \quad (15)$$

$$\left.\frac{\partial\Theta_H}{\partial r}\right|_{r=1}=\frac{1}{2} \quad 0\leqslant x\leqslant\infty; \quad (16)$$

uniform wall temperature Ⓣ

$$\Theta_T(-\infty,r)=1 \quad 0\leqslant r\leqslant 1 \quad (17)$$

$$\left.\frac{\partial\Theta_T}{\partial x}\right|_{x=\infty}=0 \quad 0\leqslant r\leqslant 1 \quad (18)$$

$$\Theta_T(x,1)=0 \quad 0\leqslant x\leqslant\infty. \quad (19)$$

And, for both thermal boundary conditions:

$$\left.\frac{\partial\Theta}{\partial r}\right|_{r=1}=0 \quad -\infty\leqslant x<0 \quad (20)$$

$$\left.\frac{\partial\Theta}{\partial r}\right|_{r=0}=0 \quad -\infty\leqslant x\leqslant\infty. \quad (21)$$

In the above relations, the axial coordinate is made dimensionless by the same reference length as the radial one, i.e. the radius of the tube. Nevertheless, the following dimensionless axial coordinates are appropriate for the presentation and analysis of the entry region results:

for isothermal flow

$$x^+=\frac{x'}{2R\,Re};$$

for non-isothermal flow

$$x^*=\frac{x'}{2R\,Pe}.$$

In the solution of the simultaneously developing laminar flow problem, the following dimensionless groups are of most interest:

the apparent Fanning friction factor

$$f_{app}(x^+)=\frac{\bar{p}(-\infty)-\bar{p}(x^+)}{4Re\,x^+}; \quad (22)$$

the mean Fanning friction factor in the hydrodynamic entrance region

$$f_m(x^+)=-\frac{1}{x^+}\frac{4}{Re}\int_0^{x^+}\left.\frac{\partial u}{\partial r}\right|_{r=1}d\xi^+; \quad (23)$$

the momentum flux correction factor

$$k_d(x^+)=2\int_0^1 u^2 r\,dr; \quad (24)$$

the pressure correction factor

$$C=(f_{app}\,Re-16)4L_{hy}^+ \quad (25)$$

where L_{hy}^+ is the dimensionless hydrodynamic entrance length, defined as the dimensionless axial position at which the centreline velocity reaches 99% of its fully developed value;

the fluid bulk temperature

$$\Theta_{fb}=\int_0^1\Theta ur\,dr\Big/\int_0^1 ur\,dr; \quad (26)$$

the local Nusselt number

$$Nu_x=2\left.\frac{\partial\Theta}{\partial r}\right|_{r=1}\Big/(\Theta_w-\Theta_{fb}). \quad (27)$$

A further relevant parameter is the dimensionless thermal entrance length, L_{th}^*, which is defined as the dimensionless axial position at which the local Nusselt number achieves the value $1.05Nu_{fd}$.

The parameters defined by relations (22)–(24) appear in the macroscopic balance equation of axial momentum for the control volume included between the tube wall and the cross-sections $x^+=-\infty$ and x^+. This balance gives

$$f_{app}\,Re=f_m\,Re+\frac{1}{2x^+}(K_d-1)+\frac{1}{2x^+}K_a \quad (28)$$

where K_a is the momentum axial diffusion correction factor

$$K_a(x^+)=-\frac{2}{Re^2}\int_0^1\frac{\partial u}{\partial x^+}r\,dr. \quad (29)$$

According to the momentum theorem, the left-hand side of equation (28) represents the resultant of all external forces acting in the axial direction on the control surface—that is, the pressure acting on the two boundary cross-sections. The right-hand side represents the rate of creation of axial momentum inside the control volume, that is, outflow minus inflow of axial momentum: the first term represents the axial momentum diffusing in the radial direction across the wall of the real tube, the second represents the axial momentum convected across the circular sections x^+ and $x^+ = -\infty$ and the third represents the axial momentum diffusing in the axial direction across the circular section x^+, the axial gradient of the axial velocity component vanishing at $x^+ = -\infty$.

SOLUTION METHODOLOGY

Conservation equations (1)–(4) with boundary conditions (5)–(21) have been solved numerically by the finite element method. The problem is reformulated by the weighted residuals Galerkin method, which Finlayson and Scriven [23] have shown to be the most straightforward in the variational formulation of transport problems. In the Galerkin method, the unknown fields u, v, p and Θ are approximated as linear combinations of trial functions $\tilde{u}$, $\tilde{v}$, $\tilde{p}$ and $\tilde{\Theta}$ which do not exactly satisfy the conservation equations but give residuals, $\mathbf{R}$. The unknown coefficients in these linear combinations are determined by the need for the residuals to be orthogonal to each of the respective trial functions, that is

$$\int_v \mathbf{R}_c \tilde{p}\, dV = 0 \tag{30}$$

$$\int_v \mathbf{R}_{mx} \tilde{u}\, dV = 0 \tag{31}$$

$$\int_v \mathbf{R}_{mr} \tilde{v}\, dV = 0 \tag{32}$$

$$\int_v \mathbf{R}_e \tilde{\Theta}\, dV = 0. \tag{33}$$

By expanding the residuals and integrating by parts those integrals that have second-order partial derivatives, the equations on which the method is based are as follows:

$$\int_v \left(\frac{\partial u}{\partial x} + \frac{\partial v}{\partial r} + \frac{v}{r}\right)\tilde{p}\, dV = 0 \tag{34}$$

$$\int_v \left\{\left(u\frac{\partial u}{\partial x} + v\frac{\partial u}{\partial r} + \frac{1}{2}\frac{\partial p}{\partial x}\right)\tilde{u} + \frac{2}{Re}\left(\frac{\partial u}{\partial r}\frac{\partial \tilde{u}}{\partial r} + \frac{\partial u}{\partial x}\frac{\partial \tilde{u}}{\partial x}\right)\right\} dV = \int_s \frac{2}{Re}\frac{\partial u}{\partial n}\tilde{u}\, dS \tag{35}$$

$$\int_v \left\{\left(u\frac{\partial v}{\partial x} + v\frac{\partial v}{\partial r} + \frac{2}{Re}\frac{v}{r^2} + \frac{1}{2}\frac{\partial p}{\partial r}\right)\tilde{v} + \frac{2}{Re}\left(\frac{\partial v}{\partial r}\frac{\partial \tilde{v}}{\partial r} + \frac{\partial v}{\partial x}\frac{\partial \tilde{v}}{\partial x}\right)\right\} dV = \int_s \frac{2}{Re}\frac{\partial v}{\partial n}\tilde{v}\, dS \tag{36}$$

$$\int_v \left\{\left(u\frac{\partial \Theta}{\partial x} + v\frac{\partial \Theta}{\partial r}\right)\tilde{\Theta} + \frac{2}{Pe}\left(\frac{\partial \Theta}{\partial x}\frac{\partial \tilde{\Theta}}{\partial x} + \frac{\partial \Theta}{\partial r}\frac{\partial \tilde{\Theta}}{\partial r}\right)\right\} dV = \int_s \frac{2}{Pe}\frac{\partial \Theta}{\partial n}\tilde{\Theta}\, dS \tag{37}$$

where, now, u, v, p and Θ are the approximate fields of velocity, pressure and temperature. A characteristic feature of the method is the insertion of the boundary conditions. Adopting the terminology of the calculus of variations, boundary conditions (6), (9), (11), (15), (16), (18), (20) and (21) enter the formulation as natural boundary conditions, being included in the surface integrals which appear on the right-hand side of equations (35)–(37), while the essential boundary conditions (5), (7), (8), (10), (12)–(14), (17) and (19) must be set directly in the solving system. In the application of the finite element method, equations (34)–(37) give a system of algebraic equations the unknowns of which are the values that the unknown functions assume at the nodal points of the discretization.

In the present analysis the finite element discretization of the integration domain is obtained by axisymmetric elements having triangular cross-sections. The axial spacing is increased logarithmically with the dimensionless coordinate in order to achieve greater accuracy near the tube entrance. Each decade is then subdivided into a constant number of elements starting from x^+ or $x^* = 0.00001$ for the downstream tube; in the upstream one the discretization is symmetric with respect to the origin. The mesh becomes thicker and thicker near the wall, owing to the strong radial gradients of both velocity and temperature inside the hydrodynamic and thermal boundary layers. Mixed interpolation is adopted following the recommendation of Jackson and Cliffe [24]: in each element the velocity components and temperature are approximated by quadratic polynomials, and the pressure by linear polynomials. In this way the velocity components and temperature are each interpolated through six nodes located at the triangle vertices and their midsides; the pressure is interpolated only through the vertex nodes. The volume and surface integrals which appear in equations (34)–(37) are computed analytically, expanding the integrand in area coordinates [25]. Neglecting the fluid property variation with temperature allows the hydrodynamic problem to be solved independently of the thermal one. Therefore, the system of non-linear algebraic equations derived from equations (34)–(36) has been solved first: from the domain subdivision into 1296 elements with 2713 nodal points one obtains a system of 5819 non-linear algebraic equations the matrix of

which has a semiband width of 111. This system has been solved iteratively by a library subroutine; at each iteration the non-linear convective terms in the momentum equation are linearized by the values obtained in the previous step. At the start of the iteration process the radial velocity component is zero everywhere; the axial component is 1 everywhere except at the real tube wall, where it vanishes. As a convergence criterion it was required that the variation of any nodal value was less than 0.01% in two successive iterations. In all the cases considered, the convergence was achieved with not more than 15 iterations. Substitution of the computed velocity field in the system of linear algebraic equations which is derived from the energy equation allows the temperature field to be solved. Computation of the surface integrals appearing in equations (35)–(37) is needed only for the elements having a portion of the boundary in common with the domain boundary, on which a condition of non-vanishing momentum or heat diffusive flux is required. After solving the system of equations (34)–(37) with boundary conditions (5)–(21), the nodal values were inserted in the left-hand side of equations (35)–(37) to compute the diffusive fluxes across the surfaces of interest. In this case, too, all the integrals have been computed analytically as well as those needed to compute the considered parameters.

A few analytical solutions may be found in the literature to compare the present numerical one. For the hydrodynamic entrance problem no exact analytical solution has been obtained, while an analytical solution of the thermal entrance problem without inclusion of axial heat diffusion has been tabulated by Shah and London [1] for the Ⓗ and Ⓣ (Graetz problem) boundary conditions. Comparison with the local Nusselt number tabulated in ref. [1] shows an approximation for the numerical solution of the energy equation better than 0.25% for every $x^* > 0.00001$, for the Ⓗ boundary condition; in the case of the Ⓣ boundary condition the approximation is not so good, being better than 0.5% for $x^* > 0.0001$ and better than 1% for $x^* > 0.00005$. For the second boundary condition the axial positions far downstream are excluded from the comparison, the local Nusselt number being computed as a ratio of wall heat flux and wall to fluid temperature difference, both vanishing near the end of the entrance section. For isothermal flow and for the more general case of simultaneously developing flow, further comparisons with experimental data and theoretical solutions are discussed in the next sections.

ISOTHERMAL FLOW RESULTS

The system of equations (34)–(36) has been solved for the following Reynolds numbers: 1, 5, 50, 150, 500 and 1000. The value 1000 may be assumed to be the limit for which, far from the immediate entrance, the solution coincides with that obtained inside the boundary layer idealization, which is independent of the Reynolds number, being similar in the r and x^+ coordinates.

The radial distribution of the axial velocity component is shown in Fig. 1 for various upstream and downstream x^+ values. At low Re, the upstream diffusion of momentum causes considerable development of the velocity profile inside the stream tube. For $Re \geqslant 150$ the axial velocity profiles have a local minimum on the tube centreline and symmetrically located maxima on either side of it. This non-monotonic radial trend, which never appears at the lower Re values considered ($Re \leqslant 50$), is referred to as velocity overshoot. Velocity overshoots are present in the downstream tube within a well-defined axial interval which shifts towards the entrance as Re increases. By comparing the nodal values (without interpolation between them) the maximum increment of the axial velocity component as a percentage of the centreline value, Δ_{max}, has been obtained; the Δ_{max} values and the axial and radial positions where they take place are presented in Table 1 as a function of Re. Vrentas *et al.* [2] solved the complete conservation equations for a maximum Re value of 250; for $Re > 50$ they observe the same effect but with the maximum velocity never more than 0.05% higher than the centreline velocity. Christiansen *et al.* [3] numerically analysed the laminar isothermal flow through an abrupt contraction. For Re values up to 500 they also present results for the circular tube of constant cross-section, assuming the stream tube–real tube model, while finding stability problems in the solution for $Re > 100$. At relatively high Re they found a concavity in the entrance-velocity profile, but with an increment of the axial velocity over the centreline value of a few tenths of 1%. The velocity increments observed in the latter two works are low by comparison with the values presented in Table 1. Nevertheless, an exact comparison is not possible because these investigators do not specify the x^+ and Re values at which the velocity overshoots were observed. It seems, however, that they observed this effect at relatively low Re values at which, owing to the axial diffusion of momentum, the concavity in the axial velocity profile is less evident.

This effect is also clearly shown by the experimental results of Burke and Berman [26]. At $Re = 108$, 206 and 340 they found the velocity overshoots for x^+

Table 1. Maximum increment of the axial velocity component as a percentage of the centreline value, Δ_{max}, and axial and radial position where it takes place, for different Reynolds numbers

	Re		
	150	500	1000
x^+_{max}	0.002	0.0005	0.0002
r_{max}	0.45	0.70	0.85
Δ_{max}	1.1	2.1	2.1

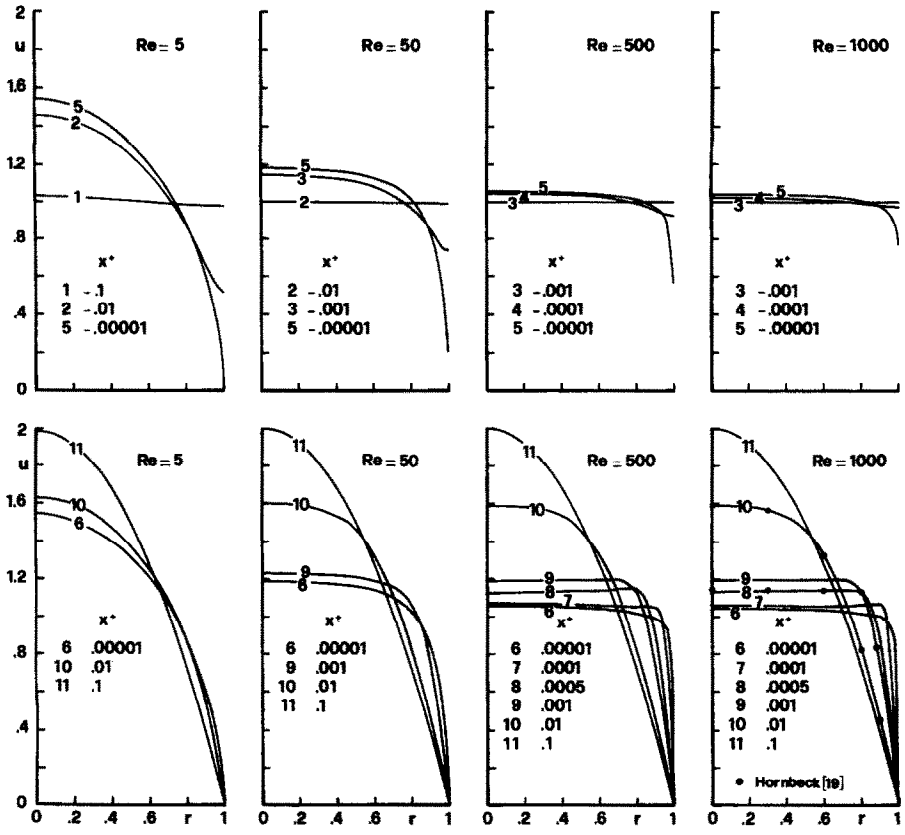

FIG. 1. Developing axial velocity profiles.

between 0 and 0.00075, with the maximum increment of the axial velocity over the centreline value up to 5.2%. At the highest Reynolds number value, where the precision of the x^+ measurement is best, the maximum increment happens at $x^+ = 0.00045$. The Burke and Berman results are not directly comparable with the present ones because of differences in the entrance conditions; however, the axial position and the order of magnitude of the maximum increment both essentially agree with the values presented in Table 1.

In Fig. 1 the boundary layer solution of Hornbeck [19] is also shown; comparison shows that at high Reynolds numbers and far from the immediate entrance, the boundary layer approximation gives axial velocity distributions in fairly good agreement with the solution of the complete momentum equation, while masking the characteristic feature just discussed.

The computed apparent Fanning friction factor–Reynolds number product distributions are shown in Fig. 2 for different Reynolds numbers; $f_{app}\,Re$ decreases as x^+ increases and increases as Re decreases without showing the different trends evident in the Schmidt and Zeldin results. However, it must be pointed out that their solution requires irrotational velocity with the uniform axial component at $x^+ = 0$. In the same figure, the Hornbeck boundary layer solution [19] is also shown; far from the immediate entrance it practically coincides with the present one for high Reynolds numbers.

In Fig. 3 the terms appearing on the right-hand side of the axial momentum balance equation (28), the sum of which equals $f_{app}\,Re$, are shown as a function of x^+. At high x^+ values ($x^+ > 0.005$), the total pressure drop from $-\infty$ to x^+ is mainly due to skin friction, the term $f_m\,Re$ prevailing over the others for every Reynolds number considered. Near the entrance, a considerable portion of the total pressure drop is due to the change in the shape of the velocity profile; at relatively high Re ($Re > 5$), the term accounting for momentum convective transport, $(K_d - 1)/(2x^+)$, prevails over that accounting for axial diffusive transport, $K_a/(2x^+)$, this not being negligible only at low Re ($Re < 50$).

The dimensionless hydrodynamic entrance length and the pressure correction factor are presented in Table 2 with the corresponding values obtained by Christiansen *et al.* [3] and by Vrentas *et al.* [2]. At $Re = 150$ and higher, L_{hy}^+ coincides with the value quoted in ref. [3] as obtained numerically by Christiansen and Lemmon [27] through simplifying the conservation equations on the basis of the boundary layer assumptions. For $Re \leqslant 150$, the present L_{hy}^+ is always considerably longer than the values of

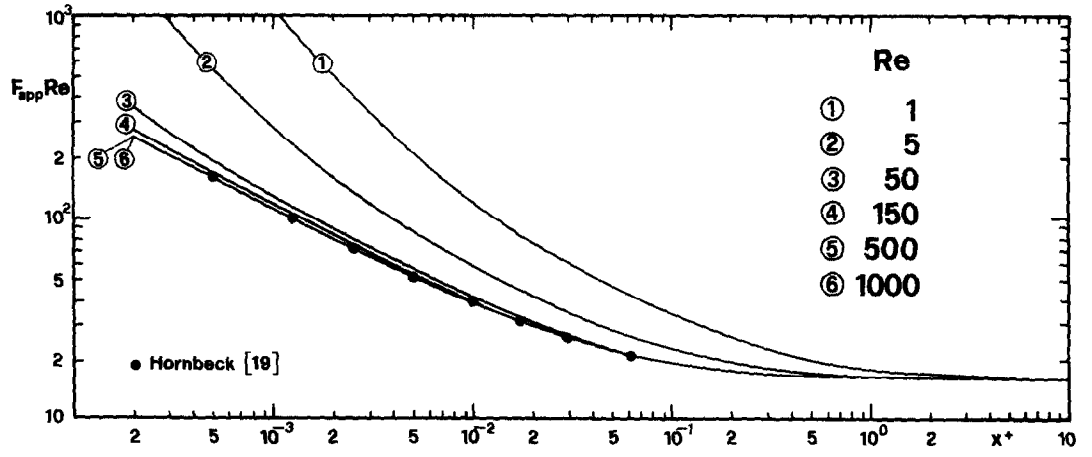

FIG. 2. Apparent Fanning friction factor–Reynolds number product for developing laminar flow.

Christiansen *et al.* and Vrentas *et al.* Both these teams of investigators solved vorticiy–transport equations by a numerical procedure using relaxation to obtain the values quoted in Table 2. However, Christiansen *et al.* [3] obtained L_{hy}^+ values 2–10% longer by solving the same problem with a different numerical method (fourth-order stream-function equations solved by relaxation).

The pressure correction factor values obtained in the present work are, for every *Re*, higher than those presented in ref. [3], which do not agree either with the corresponding values of Vrentas *et al.* [2]. As *Re* increases, the pressure correction factor decreases monotonically to the value quoted in ref. [3], as obtained in the boundary layer solution of Christiansen and Lemmon [27].

NON-ISOTHERMAL FLOW RESULTS

In the case of a non-isothermal fluid, the problem considered is of simultaneously developing flow with axial diffusion of both momentum and heat. The dimensionless group to account for axial heat diffusion is the Péclet number. With the aim of pointing out the effects of axial diffusive transport, results for $Pr = 0.7$ and different *Re* values—that is, different

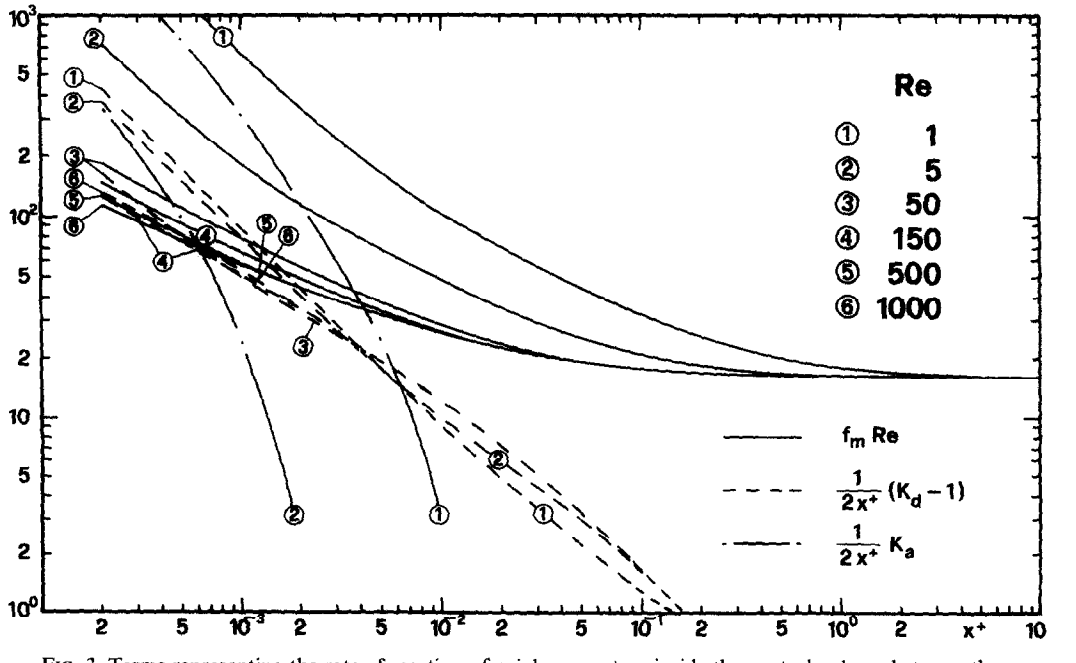

FIG. 3. Terms representing the rate of creation of axial momentum inside the control volume between the tube wall and the cross-sections $x^+ = -\infty$ and x^+, according to the axial momentum balance equation (28).

Table 2. Dimensionless hydrodynamic entrance length and pressure correction factor for different Reynolds numbers

	L_{hy}^+			C		
Re	Present solution	Ref. [3]	Ref. [2]	Present solution	Ref. [3]	Ref. [2]
1	0.385	0.333	0.33	8.77	6.82	7.76
5	0.095	0.086		2.53	2.22	
50	0.054	0.050	0.047	1.34	1.27	1.40
150	0.055	0.050	0.048	1.28	1.23	1.36
500	0.055	0.056		1.26	1.23	
1000	0.055			1.26		

Pe values—are first presented and analysed in detail. The analysis is then extended to different *Pr* values.

The graphical results for $Pr = 0.7$ are shown in Figs. 4–9. The dashed lines refer to the case of negligible axial heat diffusion, obtained by setting the second partial derivative in the axial direction to zero in equation (4). Therefore, the shifting of the dashed line from the full line shows the effect of axial heat diffusion, while the shifting between the dashed lines shows the effect of momentum axial diffusion and radial pressure gradient.

Fluid temperature distributions presented in Figs. 4 and 5 show the predevelopment of the temperature profile caused by axial heat diffusion at low *Pe*. At $Pe = 3.5$ the effect of axial heat diffusion is marked for both boundary conditions; at $Pe = 35$ it is still evident, particularly near to the entrance, while at the highest *Pe* the axial heat diffusion is ineffective.

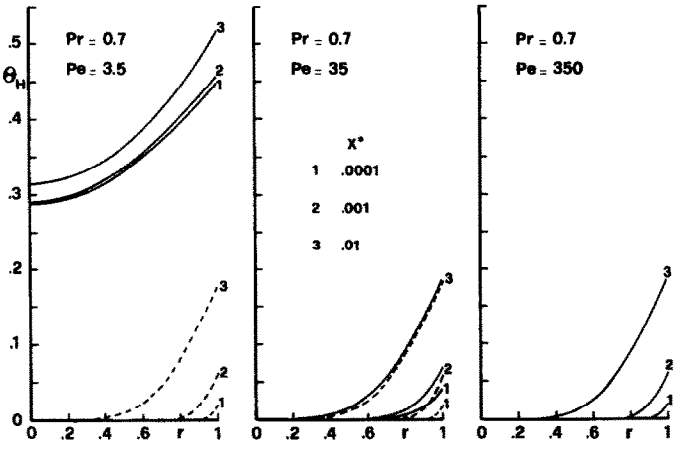

FIG. 4. Developing temperature profiles for the ⓗ thermal boundary condition: ——, axial heat diffusion included; – – –, axial heat diffusion neglected.

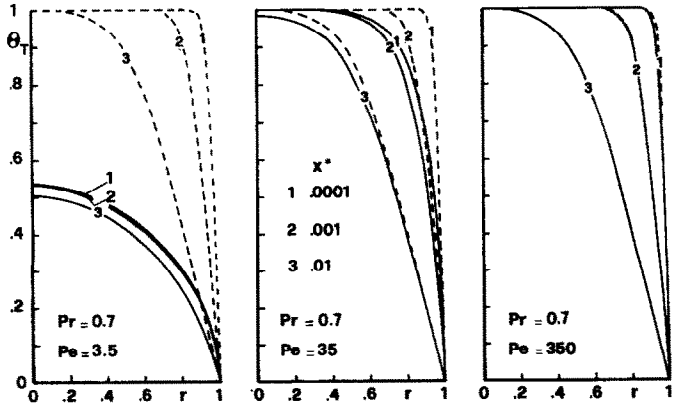

FIG. 5. Developing temperature profiles for the ⓣ thermal boundary condition: ——, axial heat diffusion included; – – –, axial heat diffusion neglected.

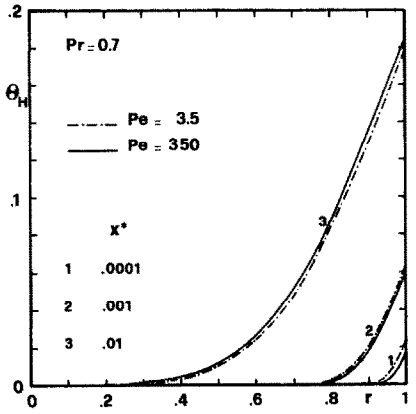

FIG. 6. Developing temperature profiles for the ⓗ thermal boundary condition, obtained by solving the complete momentum equation while neglecting axial heat diffusion.

Nevertheless, some minor effect persists at $Pe = 350$ for the ⓣ boundary condition. For the ⓗ boundary condition, the curves obtained by neglecting axial heat conduction are compared in Fig. 6, limited to the highest and lowest Pe values. Near the entrance ($x^* \leqslant 0.001$), momentum axial diffusion and the radial pressure gradient cause the fluid temperature to increase at low Re, while showing the opposite effect further downstream ($x^* = 0.01$). The reason for this behaviour can be easily explained as follows. The heat entering the flow is specified at the boundary and, in the absence of axial heat diffusion, the fluid bulk temperature for every x^* is specified too. The curves of Fig. 1 show that near the entrance, as Re increases, the axial velocity component increases near the wall; further downstream the same curves show the opposite behaviour, the axial velocity component being higher near the wall at low Re. From equation (26) it follows that to an increase of the velocity axial component near the wall, where the thermal boundary layer is developing, there must be a corresponding decrease in the fluid temperature, and vice versa, to ensure that the fluid bulk temperature is constant with x^*.

For the ⓣ boundary condition, the effect of different velocity profile developments at different Re values is shown by the fluid bulk temperature distributions presented in Fig. 7. Dashed lines show that the momentum axial diffusion lowers the efficiency of the heat transfer process near the entrance. In case ⓗ, the fluid bulk temperature distribution is the same for different Pe values, when axial heat diffusion is neglected; in Fig. 7, the curve pertinent to this case is indistinguishable from the full line relative to $Pe = 350$ which, for $x^* > 0.01$, is indistinguishable from that obtained for $Pe = 35$. On the other hand, in case ⓣ axial heat diffusion produces perceptible modifications in the fluid bulk temperature also at the highest Pe value, confirming that in the thermal entrance problem, axial heat diffusion is more effective

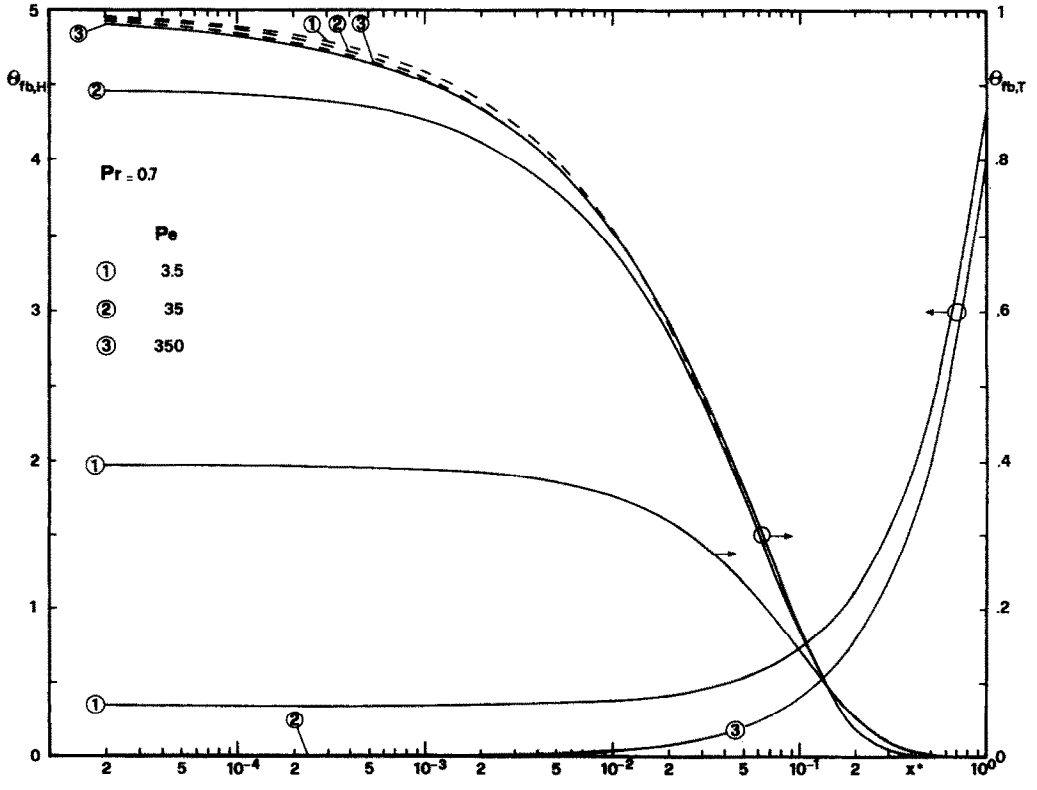

FIG. 7. Fluid bulk temperature: ——, axial heat diffusion included; – – –, axial heat diffusion neglected.

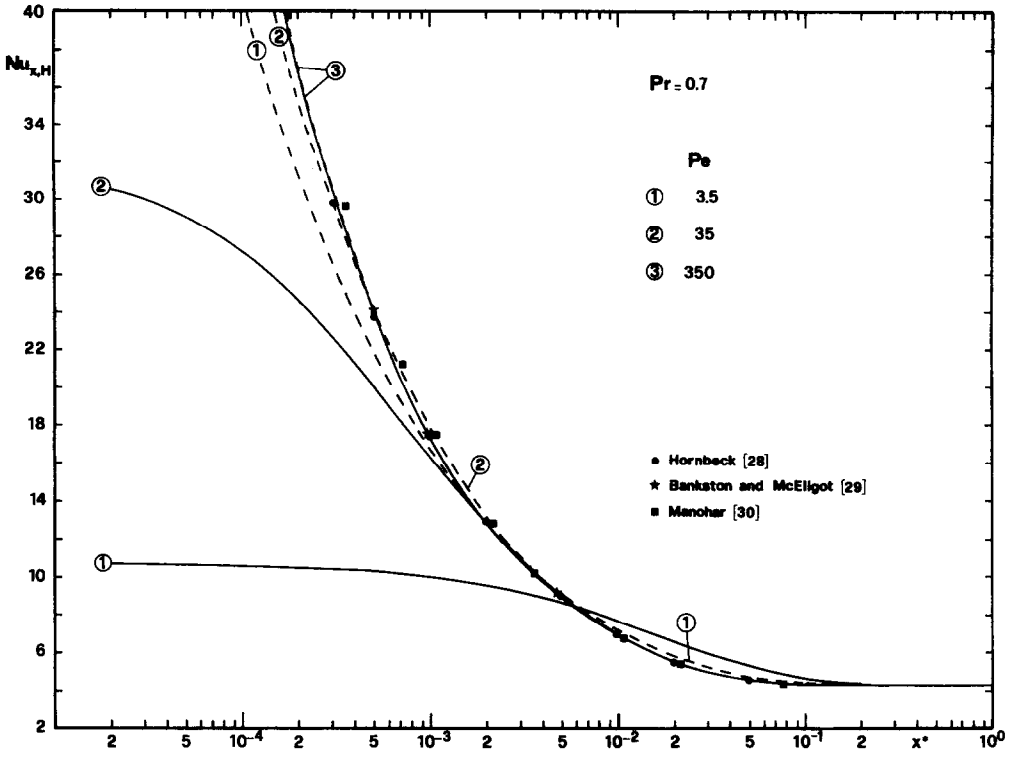

FIG. 8. Local Nusselt number for the Ⓗ thermal boundary condition ($Pr = 0.7$): ——, axial heat diffusion included; – – –, axial heat diffusion neglected.

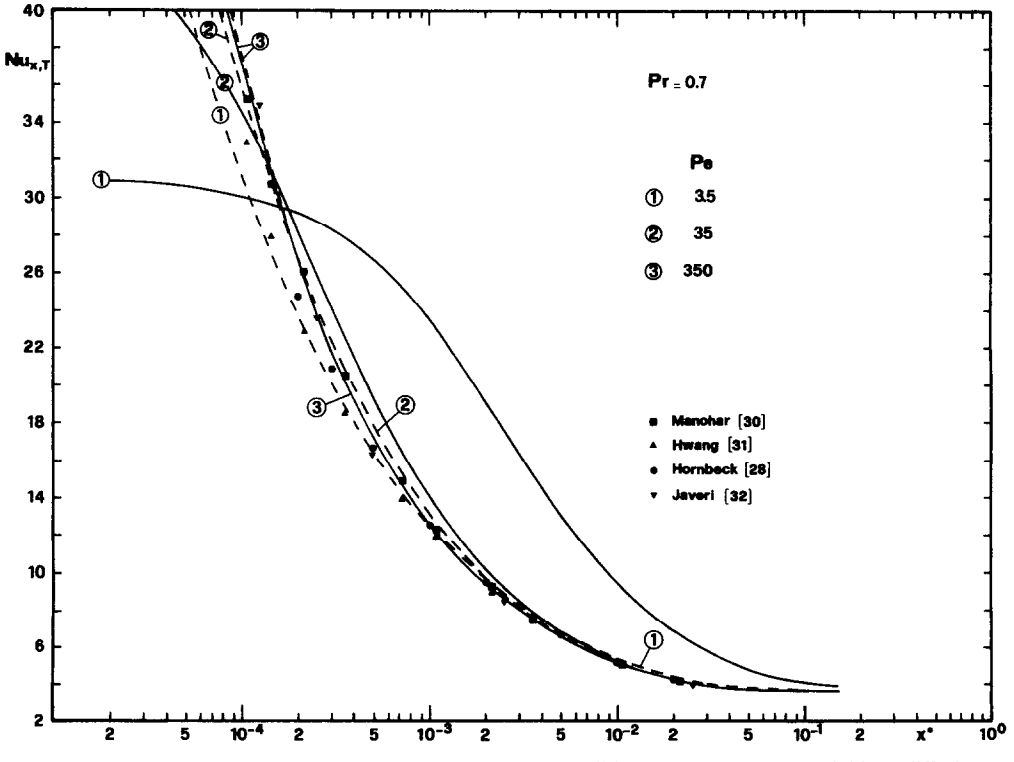

FIG. 9. Local Nusselt number for the Ⓣ thermal boundary condition ($Pr = 0.7$): ——, axial heat diffusion included; – – –, axial heat diffusion neglected.

in the case of the Ⓣ than in that of the Ⓗ boundary condition. For both thermal boundary conditions, the fluid bulk temperature at the entrance may differ considerably from the value far upstream, the effect of momentum axial diffusion and the radial pressure gradient being masked by the axial heat diffusion at low Pe values.

The local Nusselt number distributions are shown in Figs. 8 and 9. For both thermal boundary conditions, the considered higher-order effects cause, on the whole, a decrease in Nu_x near the entrance and an increase further downstream, such behaviour being shown also by the solution obtained when neglecting axial heat diffusion (dashed lines). This last effect can be easily explained, at least in case Ⓗ, on the basis of temperature and axial velocity profiles. If heat flux is specified at the boundary, in the absence of axial heat diffusion, Nu_x depends on the wall temperature only, which, as shown in Fig. 6, increases at low Re near the entrance and decreases further downstream, producing opposite behaviour in Nu_x. Even if at $Re = 500$ some effect of momentum axial diffusion and radial pressure gradient still persists, the dashed line obtained for $Pe = 350$ can be assumed to be the limit solution with which solutions incorporating the boundary layer approximation can be compared. In Fig. 8, the numerical solutions of Hornbeck [28] and Bankston and McEligot [29] compare favourably with the present one for every x^*, while that of Manohar [30], as tabulated in ref. [1], is sometimes higher. Sample points representing the numerical solutions of Manohar [30] and Hwang [31], as tabulated in ref. [1], as well as the numerical solution of Hornbeck [28] and the analytical one of Javeri [32], are plotted in Fig. 9. All of these are in close agreement with the present finite element solution at high x^* ($x^* > 0.001$), while the $Nu_{x,T}$ of Hornbeck and, in particular, of Hwang are lower near the entrance.

Distributions of Nu_x for different Pr values are shown in Figs. 10 and 11 for Ⓗ and Ⓣ thermal boundary conditions, respectively. Curves refer to various Pe values for Re ranging from 5 to 500. The Nu_x distributions for thermally developing and hydrodynamically developed flow (Poiseuille velocity profile) are also shown in the same figures (dashed lines). The solution of the thermal entry problem obtained by Hennecke [6] by accounting for axial heat diffusion compares favourably with the present solution in Fig. 10. In the case of the Ⓣ boundary condition, the hydrodynamically developed flow results at low Pe show a trend towards a uniform $Nu_{x,T}$ limit value near the entrance, in agreement with the results of Tan and Hsu [13]. Their $Nu_{x,T}$, shown in Fig. 11 for $Pe = 3$ and 5, is, however, lower near the entrance and higher further downstream. The Nu_x distributions obtained by Verhoff and Fisher [7] for $Pe = 5$ and by Michelsen and Villadsen [15] for $Pe = 3$ are also shown in the same figure. At low x^* values, they are higher than the present solution, the local Nusselt number obtained by Michelsen and Villadsen being unbounded at the entrance. In agreement with the results of Papoutsakis' analytical analysis [16], at low Pe values Nu_x approaches a finite value at the entrance for both thermal boundary conditions. The curves of Figs. 10 and 11 confirm that this is true also in the case of simultaneously developing flow; at greater Pe or at lower Pr, Nu_x decreases near the entrance, or also shows the trend towards a finite value which is, however, not reached within the interval considered for the abscissa. Further downstream, the local Nusselt number increases as Pe decreases, the effect of axial heat diffusion being greater for the Ⓣ than for the Ⓗ boundary condition. Curves referring to hydrodynamically developed flow confirm the existence of a common intersection point near $x^* = 0.075$ for the Ⓗ boundary condition. For simultaneously developing flow, a common intersection is no longer found, while for the Ⓣ boundary condition, the common intersection point is not present even for hydrodynamically developed flow. The effect of the developing velocity profile is also clearly shown by the results. With Pe being constant, an increase in Pr always causes a decrease in Nu_x; a similar effect is due to the momentum axial diffusion owing to the predevelopment in the velocity profile. For the Ⓗ boundary condition, all the curves go asymptotically to a value of 4.3636, whereas in the case of the Ⓣ boundary condition the limiting value depends on Pe.

The dimensionless thermal entrance length is presented in Table 3 for the cases analysed. For $Pr = 0.7$, the values obtained by neglecting axial heat diffusion ($k_x = 0$) are also presented in Table 4. In this case the dependence of L^*_{th} on Pe is exclusively due to momentum axial diffusion, which at $Pe = 3.5$ ($Re = 5$) produces an increment in L^*_{th} of about 31 and 29% for conditions Ⓗ and Ⓣ, respectively, while being practically ineffective at $Pe = 35$ ($Re = 50$). Neglecting axial heat diffusion, Shah [33] analytically obtained the following values for the hydrodynamically developed flow: $L^*_{th,H} = 0.043$ and $L^*_{th,T} = 0.033$. For simultaneously developing flow with $Pr = 0.7$, Shah and London [1] suggest the value $L^*_{th,H} = 0.053$ based on the $Nu_{x,H}$ of Bankston and McEligot [29], and the value $L^*_{th,T} = 0.037$ based on the values of $Nu_{x,T}$ of both Manohar [30] and Hwang [31]. Of particular significance is the comparison between the present numerical solution and the analytical one for hydrodynamically developed flow without inclusion of axial heat diffusion; for the Ⓗ boundary condition, the values are the same, whereas for that of Ⓣ, the numerically computed value is 7.4% lower. As just pointed out, at the end of the thermal entrance the approximation of $Nu_{x,T}$ deteriorates, while being better than 0.8% in the neighbourhood of the exact $L^*_{th,T}$ value (0.033). In the presence of axial heat diffusion, the thermal entrance length increases at low Pe. This effect is most noticeable at relatively high Prandtl numbers ($Pr \geq 1$), while for $Pr \ll 1$ the axial heat diffusion has less effect, the thermal entrance length being most affected by the develop-

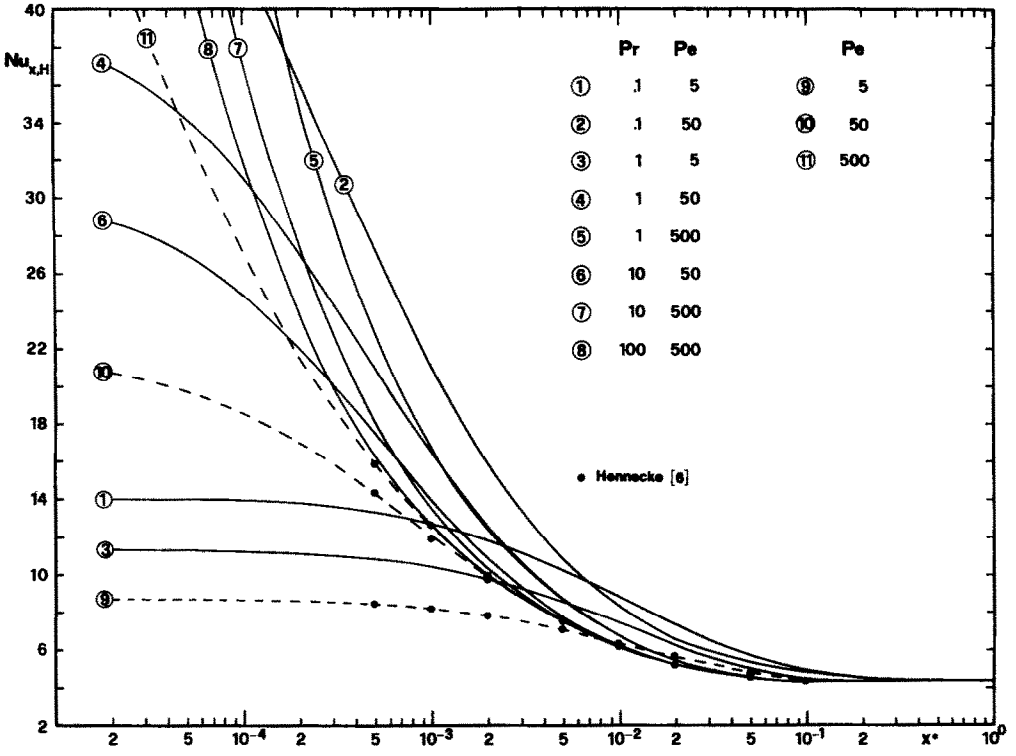

FIG. 10. Local Nusselt number for the ⑪ thermal boundary condition: ——, simultaneous development of the velocity and temperature profiles; – – –, thermally developing and hydrodynamically developed flow (Poiseuille velocity profile).

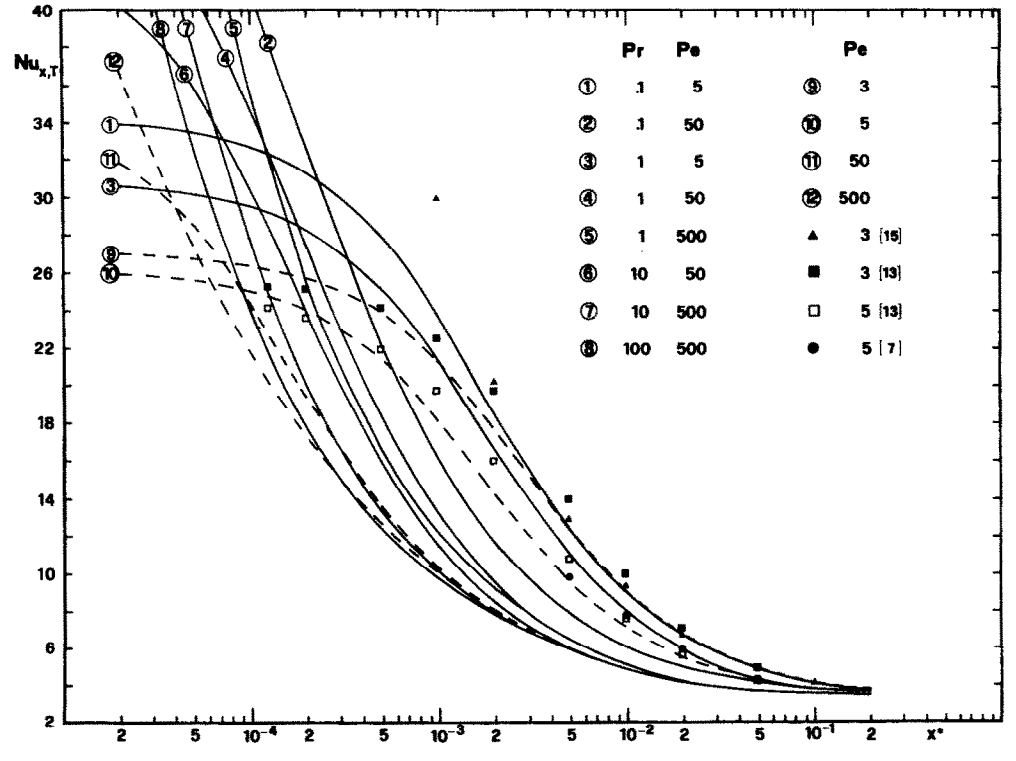

FIG. 11. Local Nusselt number for the ⑦ thermal boundary condition: ——, simultaneous development of the velocity and temperature profiles; – – –, thermally developing and hydrodynamically developed flow (Poiseuille velocity profile).

Table 3. Dimensionless thermal entrance length for the Ⓗ and Ⓣ thermal boundary conditions

	Pr					
Pe	0.1	1	10	100	Hydrodynamically developed flow	
5	0.19	0.09			0.075	Ⓗ
	0.15	0.081			0.074	Ⓣ
50	0.18	0.049	0.043		0.043	Ⓗ
	0.15	0.033	0.031		0.032	Ⓣ
500		0.048	0.043	0.043	0.043	Ⓗ
		0.033	0.031	0.031	0.031	Ⓣ

ment of the velocity profile, which is much slower than the development of the temperature profile; in this case momentum axial diffusion may affect L_{th}^* at low *Re*. On the other hand, for $Pr > 10$, the L_{th}^* values are in practice coincident with those of hydrodynamically developed flow because L_{th}^* is considerably affected by the thermal development only, much slower than the hydrodynamic one.

CONCLUDING REMARKS

The entry length problem for simultaneously developing laminar flow in a circular tube of infinite extent has been solved by the finite element numerical method. In the range of independent dimensionless parameters considered the solution never presented instabilities, thus further confirming the effectiveness of the numerical method in solving problems of simultaneous convective and diffusive transport. Comparison with the available analytical and numerical solutions and also, for isothermal flow, with experimental results showed the reliability of the approximate solution which has been presented.

Particular consideration was given to the axial diffusion of both momentum and heat, which is neglected in the boundary layer approximation. The axial momentum transfer processes have been analysed in depth, showing the relative weight of each at various Reynolds numbers. The isothermal flow results have also demonstrated the appearance, at high Reynolds numbers, of the velocity overshoots, the extent and axial position of which were found to be in acceptable agreement with the experimental results of Burke and Berman [26]. In the case of hydrodynamically developed and thermally developing flow, the results have demonstrated the effects of axial heat diffusion. The Nusselt number distributions agree with the previous solutions for the Ⓗ, but for the Ⓣ boundary condition they show an evident trend towards a limiting value near the entrance at low Péclet numbers, in agreement with both the results of Tan and Hsu [13] and the analytical analysis of Papoutsakis [16]. Similar behaviour has been shown by the simultaneously developing flow results; near the entrance Nu_x decreases and, at low Péclet and high Prandtl numbers, goes to a uniform value because of the axial diffusion of heat and, albeit to a lesser extent, of momentum. The results confirm the judgement of Papoutsakis *et al.* [12] that no global Péclet number criteria may be set for all problems concerning the inclusion of axial conduction; moreover, in simultaneously developing flow, a more general criterion should account for the Reynolds number also, the axial diffusion of momentum having a similar, though smaller, effect to that of heat.

With the aim of focusing on axial diffusion effects, fluid property variation with temperature and viscous dissipation have been disregarded in the present analysis, even though they may have a marked effect in the range for the independent dimensionless parameters considered. However, these effects can easily be included in the analysis within the scheme of the numerical procedure.

Table 4. Dimensionless thermal entrance length for the Ⓗ and Ⓣ thermal boundary conditions ($Pr = 0.7$): $k_x = 0$. axial heat diffusion neglected; $k_x \neq 0$, axial heat diffusion included

Pe	$k_x = 0$	$k_x \neq 0$	
3.5	0.068	0.116	Ⓗ
	0.045	0.109	Ⓣ
35	0.051	0.053	Ⓗ
	0.035	0.036	Ⓣ
350	0.052	0.052	Ⓗ
	0.035	0.035	Ⓣ

REFERENCES

1. R. K. Shah and A. L. London, *Laminar Flow Forced Convection in Ducts*. Academic Press, New York (1978).
2. J. S. Vrentas, J. L. Duda and K. G. Bargeron, Effect of axial diffusion of vorticity on flow development in circular conduits: part I. Numerical solutions, *A.I.Ch.E. Jl* **12,** 837–844 (1966).
3. E. B. Christiansen, S. J. Kelsey and T. R. Carter, Laminar tube flow through an abrupt contraction, *A.I.Ch.E. Jl* **18,** 372–380 (1972).
4. F. W. Schmidt and B. Zeldin, Laminar flows in inlet sections of tubes and ducts, *A.I.Ch.E. Jl* **15,** 612–614 (1969).
5. J. W. McDonald, W. E. Denny and A. F. Mills, Numerical solutions of the Navier–Stokes equations in inlet regions, *J. Appl. Mech.* **39,** 873–878 (1972).
6. D. K. Hennecke, Heat transfer by Hagen–Poiseuille flow in the thermal development region with axial conduction, *Wärme- und Stoffübertr.* **1,** 177–184 (1968).
7. F. H. Verhoff and D. P. Fisher, A numerical solution of

the Graetz problem with axial conduction included, *J. Heat Transfer* **95,** 132–134 (1973).
8. C. J. Hsu, An exact analysis of low Péclet number thermal entry region heat transfer in transversely non-uniform velocity fields, *A.I.Ch.E. Jl* **17,** 732–740 (1971).
9. E. J. Davis, Exact solutions for a class of heat and mass transfer problems, *Can. J. Chem. Engng* **51,** 562–572 (1973).
10. B. Vick, M. N. Ozisik and Y. Bayazitoglu, A method of analysis of low Péclet number thermal entry region problems with axial conduction, *Lett. Heat Mass Transfer* **7,** 235–248 (1980).
11. B. Vick and M. N. Ozisik, An exact analysis of low Péclet number heat transfer in laminar flow with axial conduction, *Lett. Heat Mass Transfer* **8,** 1–10 (1981).
12. E. Papoutsakis, D. Ramkrishna and H. C. Lim, The extended Graetz problem with prescribed wall flux, *A.I.Ch.E. Jl* **26,** 779–787 (1980).
13. C. W. Tan and C. J. Hsu, Low Péclet number mass transfer in laminar flow through circular tubes, *Int. J. Heat Mass Transfer* **15,** 2187–2201 (1972).
14. J. Newman, The Graetz problem. In *The Fundamental Principles of Current Distribution and Mass Transport in Electrochemical Cells* (Edited by A. J. Bard), Vol. 6, pp. 187–352. Dekker, New York (1973).
15. M. L. Michelsen and J. Villadsen, The Graetz problem with axial heat conduction, *Int. J. Heat Mass Transfer* **17,** 1391–1402 (1974).
16. E. Papoutsakis, Nusselt numbers near entrance of heat-exchange section in flow systems, *A.I.Ch.E. Jl* **27,** 687–689 (1981).
17. R. K. McMordie and A. F. Emery, A numerical solution for laminar-flow heat transfer in circular tubes with axial conduction and developing thermal and velocity fields, *J. Heat Transfer* **89,** 11–16 (1967).
18. H. L. Langhaar, Steady flow in the transition length of a straight tube, *J. Appl. Mech.* **9,** 55–58 (1942).
19. R. W. Hornbeck, Laminar flow in the entrance region of a pipe, *Appl. Scient. Res.* **A13,** 224–232 (1964).
20. E. B. Christiansen and S. J. Kelsey, Nonisothermal laminar contracted flow, *A.I.Ch.E. Jl* **18,** 713–720 (1972).
21. E. B. Christiansen and S. J. Kelsey, Heat transfer to non-Newtonian fluids in laminar tube entrance flow following a contraction, *PACHEC Trans.*, Part III 287–288 (1972).
22. E. Ben-Sabar and B. Caswell, A stable finite element simulation of convective transport, *Int. J. Numer. Meth. Engng* **14,** 545–565 (1979).
23. B. A. Finlayson and L. E. Scriven, On the search for variational principles, *Int. J. Heat Mass Transfer* **10,** 799–821 (1967).
24. C. P. Jackson and K. A. Cliffe, Mixed interpolation in primitive variable finite element formulations for incompressible flow, *Int. J. Numer. Meth. Engng* **17,** 1659–1688 (1981).
25. O. C. Zienkiewicz, *The Finite Element Method.* McGraw-Hill, London (1977).
26. J. P. Burke and N. S. Berman, Entrance flow development in circular tubes at small axial distances, ASME Paper 69-WA/FE-13 (1969).
27. E. B. Christiansen and H. E. Lemmon, Entrance region flow, *A.I.Ch.E. Jl* **11,** 995–999 (1965).
28. R. W. Hornbeck, An all-numerical method for heat transfer in the inlet of a tube, ASME Paper 65-WA/HT-36 (1965).
29. C. A. Bankston and D. M. McEligot, Turbulent and laminar heat transfer to gases with varying properties in the entry region of circular ducts, *Int. J. Heat Mass Transfer* **13,** 319–344 (1970).
30. R. Manohar, Quoted by Shah and London as a personal communication.
31. G. J. Hwang, Quoted by Shah and London as a personal communication.
32. V. Javeri, Simultaneous development of the laminar velocity and temperature fields in a circular duct for the temperature boundary condition of the third kind, *Int. J. Heat Mass Transfer* **19,** 943–949 (1976).
33. R. K. Shah, Thermal entry length solution for the circular tube and parallel plates, *Proc. 3rd Natl Heat Mass Transfer Conf.*, Indian Institute of Technology, Bombay, Vol. I, Paper HMT-11-75 (1975).

TRANSFERT DE CHALEUR EN REGIME PERMANENT LAMINAIRE DANS LA REGION D'ENTREE D'UN TUBE AVEC DIFFUSION AXIALE DE CHALEUR ET DE QUANTITE DE MOUVEMENT

Résumé—Le développement simultané des profils de vitesse et de température dans des tubes circulaires est analysé en tenant compte de la diffusion de la quantité de mouvement et de la chaleur. Le problème axisymétrique est posé sur la forme variationnelle par la méthode des éléments finis. Les résultats obtenus dans le cas des effets de diffusion axiale négligeables se comparent bien avec les solutions antérieures; en présence de diffusion axiale les solutions déjà connues sont dispensées et ne s'accordent pas toujours. Les résultats de l'écoulement isotherme présentés pour des nombres de Reynolds entre 1 et 1000, montrent l'aspect d'un dépassement dans les profils de vitesse axiale et aussi la dépendance, vis-à-vis de la coordonnée axiale, du nombre de Reynolds et des mécanismes de transfert axial de quantité de mouvement, de diffusion radiale à la paroi, de la convection et de la diffusion axiale. Les résultats de l'écoulement non isotherme présentés pour un nombre de Prandtl variant entre 0,1 et 100 et pour un nombre de Péclet entre 5 et 500, mettent en valeur l'effet de la diffusion axiale de quantité de mouvement et de chaleur sur la convection thermique.

STATIONÄRER LAMINARER WÄRMEÜBERGANG MIT AXIALEM WÄRME- UND IMPULSTRANSPORT IM EINLAUFBEREICH VON KREISROHREN

Zusammenfassung—Die gleichzeitige Ausbildung des Temperatur- und Geschwindigkeitsprofils in Kreisrohren wird unter Berücksichtigung des axialen Wärme- und Impulstransports untersucht. Das achsensymmetrische Problem wird in Variationsform durch die Galerkin-Methode mit gewichteten Residuen formuliert und dann numerisch mit der Methode der Finiten Elemente gelöst. Die Ergebnisse für den Fall verschwindender axialer Transporteffekte stimmen gut mit bekannten Grenzschichtlösungen überein; bei Berücksichtigung der axialen Transporteffekte streuen die in der Literatur angegebenen Lösungen sehr und stimmen nicht immer überein. Die Ergebnisse für isotherme Strömung, dargestellt für Reynolds-Zahlen zwischen 1 und 1000, zeigen sowohl das Auftreten von Überhöhungen im axialen Geschwindigkeitsprofil, als auch die Abhängigkeit von der axialen Koordinate und von der Reynolds-Zahl der verschiedenen axialen Impulstransportvorgänge: radialer Impulstransport an der Wand, Konvektion und axialer Impulstransport. Die Ergebnisse für nichtisotherme Strömung, dargestellt für Prandtl-Zahlen zwischen 0,1 und 100 und für Péclet-Zahlen von 5 bis 500, zeigen deutlich den Einfluß des axialen Impuls- und insbesondere Wärmetransports auf den konvektiven Wärmeübergang.

СТАЦИОНАРНЫЙ ЛАМИНАРНЫЙ ТЕПЛООБМЕН НА НАЧАЛЬНОМ УЧАСТКЕ ТРУБ КРУГЛОГО СЕЧЕНИЯ С АКСИАЛЬНЫМ ПЕРЕНОСОМ ТЕПЛА И ИМПУЛЬСА

Аннотация—Анализируется совместное развитие профилей скорости и температуры в трубах круглого сечения с учетом аксиального переноса импульса и тепла. Осесимметричная задача формулируется в вариационной форме методом взвешенных разностей Галеркина, а затем решается численно методом конечных элементов. Результаты, полученные для случая пренебрежимо малых эффектов аксиальной диффузии, удовлетворительно согласуются с известными решениями для пограничного слоя; при существенной роли аксиального переноса решения недостаточно представлены в литературе и не всегда согласуются между собой. Из результатов для изотермического течения при числе Рейнольдса в диапазоне от 1 до 1000 можно сделать вывод о возникновении выбросов в профиле продольной скорости, а также зависимости различных процессов переноса импульса (радиальной пристенной диффузии, конвекции и аксиальной диффузии) от осевой координаты и числа Рейнольдса. Данные для неизотермического течения при числе Прандтля, изменяющемся от 0,1 до 100, и числах Пекле—от 5 до 500 иллюстрируют влияние аксиального переноса импульса и тепла на интенсивность конвективного теплопереноса.